JOURNAL OF CATALYSIS 155, 117–130 (1995)

# Reactivity and Physicochemical Characterisation of $V_2O_5$–$WO_3/TiO_2$ De-$NO_x$ Catalysts

Luis J. Alemany,*,[1] Luca Lietti,* Natale Ferlazzo,* Pio Forzatti,* Guido Busca,† Elio Giamello,‡ and Fiorenzo Bregani§

*Dipartimento di Chimica Industriale e Ingegneria Chimica "G. Natta," Politecnico di Milano, Piazza L. da Vinci 32, 20133 Milan; †Istituto di Chimica, Facoltà di Ingegneria, Università, Piazzale Kennedy, 16129 Genoa; ‡Dipartimento di Chimica Inorganica, Chimica Fisica e Chimica dei Materiali, Università di Torino, Turin; and §Centro Ricerche Ambiente e Materiali, ENEL-DSR Via Monfalcone 15, 20132 Milan, Italy

Received August 8, 1994; revised February 20, 1995

$V_2O_5$–$WO_3/TiO_2$ samples with compositions similar to those of commercial de-$NO_x$ catalysts ($WO_3$ ~ 9% w/w, $V_2O_5$ < 3% w/w) are characterised by XRD, surface area and pore size distribution, Fourier transform infrared, laser Raman, UV–vis diffuse reflectance, electron paramagnetic resonance spectroscopies, and catalytic tests in the reduction of $NO_x$ by $NH_3$. The $V_2O_5$–$WO_3/TiO_2$ catalysts exhibit higher reactivity than the binary $V_2O_5/TiO_2$ and $WO_3/TiO_2$ samples with the same metal loading, and the temperature window for the SCR reaction is greatly widened. The catalysts consist of anatase $TiO_2$ and their morphological properties closely resemble that of $WO_3/TiO_2$ for (V + W) surface coverages lower than one. Monomeric vanadyls and wolframyls and polymeric $W_wO_y$ groups are observed in the samples with low vanadia loadings that are apparently similar to those present on the surface of the binary oxide systems with comparable metal loadings. On increasing the vanadium loading, polyvanadate species are also formed. EPR, FTIR, FT-Raman, and UV–vis techniques indicate a strong electronic interaction between V and W oxide species at the surface of the $TiO_2$ support. This interaction leads to a higher reducibility of the ternary sample with respect to the corresponding binary ones. A synergism between V and W oxide surface species is suggested, which accounts for the high reactivity of the ternary samples in the SCR reaction. It is suggested that the higher reducibility of the samples, due to the electronic interactions between V and W and the $TiO_2$ support, is responsible for the higher reactivity of the ternary catalysts, particularly at low temperatures. 

## INTRODUCTION

$V_2O_5$–$WO_3/TiO_2$ catalysts are widely used in the selective catalytic reduction (SCR) of nitrogen oxides in power plant stack gases (1, 2).

In commercial De–$NO_x$ SCR catalysts $TiO_2$ anatase is used as a base material (~80% w/w) to support the active components. $V_2O_5$ is responsible for the activity both in the reduction of $NO_x$ (3) and in the oxidation of $SO_2$, present in glue gas, to $SO_3$ (4); the $V_2O_5$ content is generally low (<2% w/w) and is reduced below 1% w/w in high-sulphur applications to limit the concentration of $SO_3$ at the exit of the catalytic reactor. $WO_3$ provides thermal stability to the catalyst, presents a much lower activity in both denitrification and $SO_2$ oxidation reactions, and is employed in relatively large amounts (~10% w/w).

$V_2O_5/TiO_2$ catalysts have been extensively studied in the past (5–14). It has been reported that vanadia dispersed on $TiO_2$ anatase is present in the form of isolated vanadyls and polymeric $V_xO_y$ species (15–17) and that monomeric vanadyls predominate at low $V_2O_5$ loadings (15). Catalytic tests have shown that the specific activity of polymeric $V_xO_y$ species in the SCR reaction is much higher than that of monomeric vanadyl species (18, 19).

Reports are also available on the structure and reactivity of $WO_3/TiO_2$ (20–28). It has been demonstrated that: (i) $WO_3$ inhibits the initial sintering of anatase $TiO_2$ and the anatase to rutile transition; (ii) both monomeric wolframyls and polymeric $W_xO_y$ groups are present at the catalyst surface; (iii) monomeric wolframyls predominate at lower $WO_3$ loadings; (iv) tungsta imparts to the system strong Lewis and Broensted acidity; and (v) the denitrification activity of $WO_3/TiO_2$ is much lower than that of $V_2O_5/TiO_2$.

However, investigations on $V_2O_5$–$WO_3/TiO_2$ catalysts are scarce (29–35). In a preliminary study performed by using infrared and UV–vis diffuse reflectance spectroscopies it has been proposed that surface vanadium oxide and tungsten oxide species consist of mono-oxo vanadyls and wolframyls closely resembling those present in the binary oxide catalysts. Besides, $WO_3$ was reported to widen the temperature window of SCR, to increase the poison resistance to alkali metal oxides and arsenious oxide, and to reduce ammonia oxidation as well as $SO_2$ oxidation.

In this paper the reactivity in the reduction of NO by $NH_3$ and the structural, morphological, and physicochem-

[1] On leave from University of Malaga, Spain.



0021-9517/95 $12.00

ical characteristics of $V_2O_5$–$WO_3/TiO_2$ de-$NO_x$ catalysts are reported. X-ray diffraction (XRD), surface area ($S_a$) and pore size distribution measurements, electron paramagnetic resonance (EPR), UV–vis diffuse reflectance (UV–vis DR), Fourier transform infrared (FTIR), and laser Raman (LR) were employed with the purpose of clarifying the bulk, surface, acid, and redox properties of this catalytic system as compared to those of the corresponding $V_2O_5/TiO_2$ and $WO_3/TiO_2$ systems.

## METHODS

### *Catalyst Preparation*

$V_2O_5$–$WO_3/TiO_2$ catalysts were prepared by dry impregnation of $WO_3/TiO_2$ calcined at 873 K with a hot water solution of ammonium metavanadate and oxalic acid, followed by drying and calcination at 823 K for 2 h. The $V_2O_5$ content in the samples was varied between 0.3 and 3.56% w/w. Details on the preparation of the $WO_3/TiO_2$ sample have already been reported in (21). The outgassed samples were obtained by heating at 423 K under vacuum ($70 \times 10^{-3}$ Torr) for 4 h. Reference catalysts consisting of $V_2O_5/TiO_2$ with similar $V_2O_5$ weight contents were prepared as described elsewhere (21, 22). The catalysts are identified in the paper according to their $V_2O_5$ and $WO_3$ content, e.g., $V_2O_5(1.0)$–$WO_3(9)/TiO_2$ identifies a sample with $WO_3$ = 9% w/w and $V_2O_5$ = 1.0% w/w.

### *Catalytic Measurements*

Catalytic measurements have been carried out in a quartz tubular fixed bed microreactor (i.e. 7 mm) containing 160 mg catalyst. A feed consisting of ~800 ppm NO, ~800 ppm $NH_3$, and ~1% v/v of oxygen in helium was used (total flow rate = 60 N $cm^3$/min). NO conversion was measured by means of a UTI quadrupole mass spectrometer (QMS) whereas the analysis of $N_2$ and $N_2O$ was carried out by on-line GC using a poraplot Q and a 5 Å molecular sieve column in a parallel arrangement. Further details on the experimental procedure can be found elsewhere (19).

### *Characterisation of Catalysts*

Powder X-ray diffraction analyses have been performed with a Philips vertical goniometer PW 1050-70 and Ni-filtered CuK$\alpha$ radiation.

Surface area and micro- and mesopore size distribution have been determined by $N_2$ adsorption with the BET method using a Carlo Erba Sorptomatic 1800 Series instrument. Mesopore distribution measurements have been obtained by the mercury penetration method using a Carlo Erba Porosimeter 2000 Series instrument.

The FTIR spectra were recorded by a Nicolet 5ZDX FTIR spectrometer equipped with a greaseless gas manipulation/evacuation ramp, an infrared cell, and a furnace for sample heating. Both self-supporting pressed disks of pure powders and KBr pressed disks were used.

Laser-Raman spectra were recorded with a Dilor multichannel spectrometer using an argon spectra Physic Laser (514.6 nm). FT-laser-Raman spectra were also collected by using a Nicolet 910 laser Raman spectrometer (1064 nm).

The EPR spectra have been recorded in the X-band mode by a Varian E109 spectrometer operating between 9.2 and 9.5 GHz microwave frequency and with a field modulation of 100 kHz. The spectrometer was equipped with a computer interface for spectra recording and elaboration. The spectra were recorded both at room temperature and at 77 K. Varian pitch ($g$ = 2.0028) was used as a reference standard for $g$ values.

UV–vis DR spectra were obtained by using a Jasco double-beam spectrometer equipped with an integrating sphere. The outgassing of the catalysts upon heating at 423 K under vacuum ($70 \times 10^{-3}$ Torr) was followed by the recording *in situ* of the UV–vis DR spectra at r.t. A homemade cell was used for this purpose.

## RESULTS

### *1. XRD and Morphology*

To investigate the effect of tungsten on the catalyst morphological properties, ternary $V_2O_5$–$WO_3/TiO_2$ samples with different $WO_3$ (1, 3, and 9% w/w) and $V_2O_5$ (0–3.56% w/w) contents were prepared. Figure 1 reports the catalysts surface areas as a function of the (W + V) coverage. The curves reported in Fig. 1 refer to catalysts with the same $V_2O_5$ or $WO_3$ loading (solid and dotted lines, respectively). The figure clearly shows that a significant loss of surface area occurs upon $V_2O_5$ addition for the samples with low $WO_3$ loading. Indeed for the samples with $WO_3$ = 1% w/w the surface area significantly decreases on increasing the $V_2O_5$ loading up to 1.4% w/w. As shown in Fig. 1 this is not the case for the samples with high $WO_3$ loadings, for which only a limited decrease in the surface area has been observed. It can be concluded that $WO_3$ loadings of about 10% w/w are most suited to preserve the specific surface area in the ternary $V_2O_5$–$WO_3/TiO_2$ catalysts.

Samples with high $WO_3$ loadings (9% w/w) have been used for further investigations. Table 1 shows the phase composition, the mean crystal dimension ($d_{cryst}$), the surface area ($S_a$), the pore volume ($V_p$), the mean pore radius ($r_p$), and the W, V, and (W + V) surface coverages for the ternary catalysts with $WO_3$ = 9% w/w. Surface coverages have been calculated assuming a monolayer capacity of 7 micromoles/$m^2$ for $WO_3$ (36) and of 0.145% w/w for $V_2O_5/m^2$ (37). The surface coverage of (W + V) has been

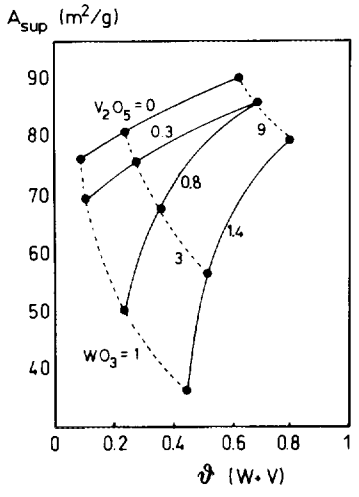


FIG. 1. Catalyst surface areas ($m^2$/g) as a function of the (V + W) coverage. Solid lines and dotted lines refer to samples with the same $V_2O_5$ and $WO_3$ loading, respectively.

estimated by summing those of W and V. From Table 1 it appears that the theoretical monolayer coverage in terms of (W + V) is approached in the samples with $V_2O_5$ = 2.56% w/w and is exceeded with $V_2O_5$ = 3.56% w/w.

All the samples with $V_2O_5 < 3.56\%$ w/w are monophasic and only the anatase polymorphic form of $TiO_2$ is detected; traces of the rutile form are detected in the catalyst with $V_2O_5$ = 3.56% w/w. No significant differences are observed in the crystallite dimensions of anatase on increasing the $V_2O_5$ content with the only exception of the sample with the highest vanadium loading where a slight growth of the particles was measured.

The morphological characteristics of the samples are modified only to a limited extent on increasing the vanadia loading up to 2.56% w/w ($S_a$ = 90–78 $m^2$/g, $V_p$ = 0.3–0.35 $cm^3$/g, $r_p$ = 50–100 Å). A more pronounced reduction in surface area (64 $m^2$/g), a slightly larger pore volume (0.38 $cm^3$/g), and a bimodal pore size distribution ($r_p$ = 70 and 200 Å) are observed in the sample with the highest vanadium loading ($V_2O_5$ = 3.56%).

On increasing the calcination temperature to 873 K no significant changes in phase composition and crystallite dimensions are detected. Only for the sample with $V_2O_5$ = 3.56% w/w are traces of $V_2O_5$ (XRD lines at $2\theta$ = 26.18°, 20.31°, and 31.06°) observed. Besides, larger crystallite dimensions of anatase $TiO_2$ (227 Å vs 173 Å) are evident. It is worth noting that $V_2O_5$ is already detected in this sample by FTIR spectroscopy after calcination at 823 K due to the higher sensitivity of this technique.

The morphological data of Table 1 indicate that vanadia affects both the initial sintering of $TiO_2$ and the anatase to rutile transformation in $V_2O_5$–$WO_3$(9)/$TiO_2$ catalysts only at high vanadia loadings ($V_2O_5$ = 2.56–3.56% w/w) that correspond to surface coverages of (W + V) close to or greater than 1. In this case the two processes mentioned above are faster, particularly at high calcination temperatures; larger dimensions of the anatase crystals are measured traces of rutile and $V_2O_5$ are detected, and a bimodal pore size distribution is observed that is associated with the incipient anatase to rutile transformation. This is consistent with the well-known promoting effect of vanadia on both the $TiO_2$ sintering and the anatase to rutile transformation.

### 2. *Catalytic Activity Measurements*

The results of catalytic tests in the reduction of NO by $NH_3$ performed over different $V_2O_5$/$WO_3$(9)/$TiO_2$ catalysts and over $V_2O_5$/$TiO_2$ and $WO_3$/$TiO_2$ samples with the same metal loadings are shown in Fig. 2.

The reactivity of the ternary catalysts is significantly higher than that of the binary samples with the same V loadings; in the presence of $WO_3$, the temperature required for 50% conversion is lowered from ~590 K to ~540 K for $V_2O_5$ = 0.78% w/w, and from ~570 K to

TABLE 1

**Structural and Morphological Data of $V_2O_5(x)$–$WO_3$(9)/$TiO_2$ Samples ($x$ = 0–3.56% w/w) Calcined at 823 K**

| $V_2O_5$ (% w/w) | 0 | 0.3 | 0.78 | 1.00 | 1.40 | 2.56 | 3.56 |
|---|---|---|---|---|---|---|---|
| Phases | A | A | A | A | A | A | A[a] |
| $d_{cryst.}$ (Å) | 155 | 140 | 144 | 146 | 140 | 140 | 173 |
| $S_a$ ($m^2$/g) | 90 | 85 | 87 | 87 | 80 | 78 | 64 |
| $V_p$ ($cm^3$/g) | 0.31 | 0.33 | 0.32 | 0.30 | 0.30 | 0.35 | 0.38 |
| $r_p$ (Å) | 55 | 65 | 70 | 70 | 70 | 100 | 70/200 |
| W coverage | 0.60 | 0.63 | 0.62 | 0.62 | 0.67 | 0.69 | 0.84 |
| V coverage | 0.00 | 0.02 | 0.06 | 0.08 | 0.12 | 0.23 | 0.38 |
| (W + V) coverage | 0.60 | 0.65 | 0.68 | 0.70 | 0.79 | 0.92 | 1.22 |

*Note.* A = anatase.
[a] Trace of rutile.

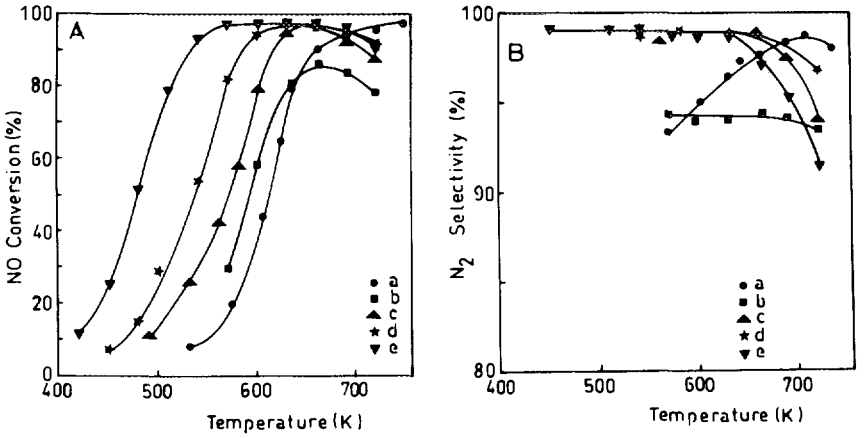


FIG. 2. NO conversion (A) and $N_2$ selectivity, defined as $[N_2]/([N_2] + [N_2O])$, (B) versus temperature over: $WO_3(9)/TiO_2$ (a), $V_2O_5(0.78)/TiO_2$ (b), $V_2O_5(1.4)/TiO_2$ (c), $V_2O_5(0.78)$–$WO_3(9)/TiO_2$ (d), and $V_2O_5(1.4)$–$WO_3(9)/TiO_2$ (e). Experimental conditions: catalyst weight, 160 mg (60–100 mesh); $P$ = 1 atm; flow rate, 60 N cm$^3$/min; feed, He + 800 ppm $NH_3$ + 800 ppm NO + ~1% $O_2$.

~480 K for $V_2O_5$ = 1.4% w/w. This clearly indicates that $WO_3$ increases the activity of $V_2O_5/TiO_2$ catalysts. Besides, the temperature window corresponding to high NO conversion and almost complete selectivity to $N_2$ is greatly amplified in the ternary catalysts since the catalysts are active at lower temperatures and high selectivites to $N_2$ are preserved in the high-temperature region.

A correspondence is always observed between the decrease in NO conversion and the decrease in $N_2$ selectivity. Lower $N_2$ selectivities are measured in the case of poorly active catalysts such as $V_2O_5(0.78)/TiO_2$ and $WO_3/TiO_2$, possibly because of the greater relative importance of the direct oxidation of ammonia.

The data have been analysed assuming an isothermal plug flow reactor model and a first-order power-law rate equation ($r = k^\circ \exp(-E_{act}/RT)\, C_{NO}$) to estimate $k^\circ$ and $E_{act}$, after verifying the absence of interphase and intraparticle diffusion limitations. Comparable values of the activation energy in the range 13–15 Kcal/mol have been calculated for $V_2O_5/TiO_2$ and $V_2O_5/WO_3(9)/TiO_2$ catalysts. In the case of $WO_3/TiO_2$ a slightly higher value of $E_{act}$ has been estimated (18 Kcal/mol). These values compare well with those reported in the literature for vanadia/titania-based catalysts, i.e., 10–15 Kcal/mol (38).

The values of the preexponential factors and of the activation energies have been used to calculate the V and W turnover frequencies (TOF, moles of NO converted $s^{-1}$ mol $V^{-1}$ or $W^{-1}$) for the binary systems (Table 2). The contribution of the exposed Ti atoms has been taken into account in the calculation of the TOFs. From Table 2 it appears that the TOFs of the vanadia/titania catalysts increase on increasing the vanadia loading (18, 19) and are much greater than those of the tungsta/titania sample, in line with the well-known higher activity of vanadia/titania as compared to tungsta/titania in the SCR reaction.

The reactivity of the ternary $V_2O_5/WO_3(9)/TiO_2$ catalysts has been tentatively described by the simple additive model

$$R_{spec} = TOF_V \times \frac{\text{moles V}}{g_{cat}} + TOF_W \times \frac{\text{moles W}}{g_{cat}}, \quad [1]$$

where $R_{spec}$ is the specific rate of reaction (moles of NO converted $s^{-1}\, g_{cat}^{-1}$). Equation [1] assumes that the specific rate of reaction of the ternary catalysts can be obtained by simple addition of the contributions of vanadia and tungsta to NO consumption. These contributions are estimated by the turnover frequencies of V and W in $V_2O_5/TiO_2$ and $WO_3/TiO_2$ catalysts with the same loadings, respectively. In Eq. [1] the reactivity of the exposed $TiO_2$ surface on NO consumption can be safely neglected.

The values of $R_{spec}$ estimated according to Eq. [1] for three different $V_2O_5$–$WO_3/TiO_2$ catalysts have been reported in Fig. 3 (filled symbols), where they are compared with the corresponding experimental ones (open sym-

TABLE 2

**Calculated Turnover Frequency (TOF, mol NO Converted $s^{-1}$ mole $V^{-1}$ or $W^{-1}$) for the Vanadia/Titania and Tungsta/Titania Catalysts**

| Catalyst | V or W coverage | Turnover frequency (TOF) | | |
|---|---|---|---|---|
| | | 500 K | 550 K | 600 K |
| $TiO_2$ | — | $0.003 \times 10^{-3}$ | $0.012 \times 10^{-3}$ | $0.040 \times 10^{-3}$ |
| $V_2O_5(0.8)/TiO_2$ | 0.09 | $0.208 \times 10^{-3}$ | $0.703 \times 10^{-3}$ | $1.926 \times 10^{-3}$ |
| $V_2O_5(1.47/TiO_2$ | 0.21 | $0.224 \times 10^{-3}$ | $0.787 \times 10^{-3}$ | $2.223 \times 10^{-3}$ |
| $V_2O_5(3.56)/TiO_2$ | 0.51 | $2.205 \times 10^{-3}$ | $6.822 \times 10^{-3}$ | $1.526 \times 10^{-2}$ |
| $WO_3(9)/TiO_2$ | 0.6 | $0.017 \times 10^{-3}$ | $0.091 \times 10^{-3}$ | $0.353 \times 10^{-3}$ |

*Note.* Assumed NO concentration = 1000 ppm.

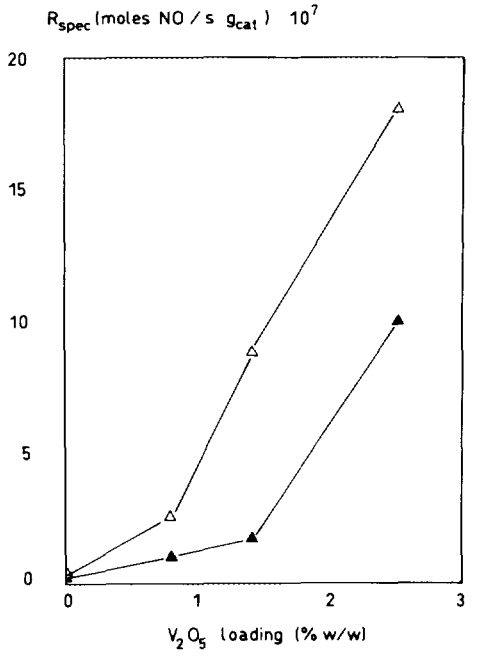


FIG. 3. Values of $R_{spec}$ (Moles NO converted $s^{-1}$ $g_{cat}^{-1}$) for $V_2O_5$ ($x$)–$WO_3(9)/TiO_2$ catalysts as a function of the $V_2O_5$ loading. $T$ = 550 K; NO = 1000 ppm. Filled symbols, calculated according to Eq. [1]; open symbols, calculated from the estimated values of the activation energy and preexponential factor.

bols). From Fig. 3 it appears that for all the investigated $V_2O_5$–$WO_3/TiO_2$ samples the specific rate of reaction is 2–4 times smaller than that measured over the same catalysts. This indicates that the reactivity of V and/or W active species in the ternary catalysts is higher than that observed over the binary samples with the same $V_2O_5$ and $WO_3$ loadings.

It has been previously reported (18, 19) that over $V_2O_5/TiO_2$ binary catalysts the vanadium TOFs increase on increasing the $V_2O_5$ coverage. This has been associated with the formation of highly active polyvanadate species. One can speculate that the presence of tungsten oxide in $V_2O_5$–$WO_3/TiO_2$ catalysts may reduce the $TiO_2$ surface area available for vanadium so that the vanadium coverage is eventually increased. This will favour the formation of polyvanadate species, thus increasing catalyst reactivity. Along these lines, calculations were also performed by assuming that $V_2O_5$ is dispersed only onto the fraction of the $TiO_2$ surface which is not covered by tungsta, and the vanadium TOF values corresponding to those new coverages have been introduced in Eq. [1]. Still the values of $R_{spec}$ estimated with Eq. [1] are lower than the corresponding experimental ones by roughly a factor of 2. This eventually indicates that the formation of polyvanadate species (if any) cannot be fully responsible for the increase in the catalytic activity which is observed by passing from the $V_2O_5/TiO_2$ catalysts to the $V_2O_5$–$WO_3/TiO_2$ samples. This is also in line with the observation that the increase in the reactivity is not accompanied by the corresponding decrease in the selectivity which is typically observed upon increasing the $V_2O_5$ loading over binary $V_2O_5/TiO_2$ samples [18, 19]. This eventually suggests the existence of a synergism between V and W in the SCR reaction. To further investigate this interaction a detailed physicochemical characterisation of the ternary samples has been undertaken and is reported in the following sections.

### *3. Electron Paramagnetic Resonance*

The ternary $V_2O_5$–$WO_3(9)/TiO_2$ catalysts exhibit an intense and well-resolved EPR spectrum both after calcination (823 K) and after reduction (annealing at 423 K). The spectrum obtained on the calcined $V_2O_5(1.0)$–$WO_3(9)/TiO_2$ sample is reported in Fig. 4a; the spectrum has been recorded after quick outgassing of the fresh samples at room temperature in order to remove the oxygen atmosphere from the EPR cell. The spectra of the $V_2O_5(0.3)$–$WO_3(9)/TiO_2$ and $V_2O_5(1.4)$–$WO_3(9)/TiO_2$ samples show basically the same profile. The spectrum of $V_2O_5(1.0)$–$WO_3(9)/TiO_2$, however, is more intense than that of $V_2O_5(0.3)$–$WO_3(9)/TiO_2$ by a factor of about 2 while that of $V_2O_5(1.4)$–$WO_3(9)/TiO_2$ is only slightly more intense than that of $V_2O_5(1.0)$–$WO_3(9)/TiO_2$. The spectrum in Fig. 4a is due to tetravalent vanadium and specifically to vanadyl $VO^{2+}$ ions (see below); this is indicated by the presence of the hyperfine structure due to the $^{51}V$ nucleus ($I$ = 7/2, multiplicity 8). The resolution of the spectrum is fairly good and indicates, however, a complex situation in that at least three families of V(IV) ions are

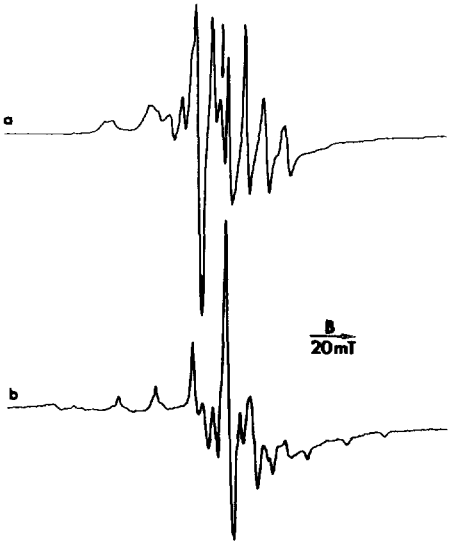


FIG. 4. EPR spectra of $V_2O_5(1.0)$–$WO_3(9)/TiO_2$ catalyst calcined at 823 K after outgassing at r.t. (a) and $V_2O_5(1.0)/TiO_2$ after outgassing at 473 K for 1 h (b). The vertical arrow indicates $g$ = 2.0028. The magnetic induction $B$ is in milliTesla (1 mT = 10 G).

present. Two of them are magnetically isolated $VO^{2+}$ ions (I and II), giving rise to structured EPR signals characterised by axial $g$ and $A$ tensors with slightly different principal values due to minor differences in the oxygen coordination. The third family consists of magnetically interacting V(IV) centers which give rise to a broad and structureless EPR line that is responsible, in the spectrum reported in Fig. 4, for the nonlinearity of the base line. The parameters obtained by a preliminary computer simulation of the experimental spectrum are as follows: species I, $g_\parallel = 1.912$, $g_\perp = 1.983$, $A_\parallel = 195$ G, and $A_\perp = 74$ G; species II, $g_\parallel = 1.905$, $g_\perp = 1.978$, $A_\parallel = 195$ G, and $A_\perp = 69$ G. The simulation also indicates that the abundance of the two families of isolated ions (I and II) is nearly the same and that the amounts of interacting ions are slightly higher than the amount of whole isolated ions.

The presence of isolated V(IV) after calcination at high temperatures is typical of $V_2O_5$–$WO_3/TiO_2$. In the case of the $V_2O_5/TiO_2$ reference system ($V_2O_5$ = 1.0% w/w) the typical vanadium EPR spectrum is visible only in the case of the reduced samples, or it appears upon the annealing of the calcined samples at $T > 423$ K (Fig. 4b). Besides, the spectra of the binary $V_2O_5/TiO_2$ samples are (for the same annealing temperature) about one order of magnitude less intense than those of the $V_2O_5$–$WO_3/TiO_2$ samples with the same vanadium loading. It can thus be concluded that the ternary samples exhibit a higher capability in stabilizing isolated tetravalent vanadium ions than the corresponding binary samples.

The third family of V(IV) ions is likely constituted by vanadylic groups which, in comparison with the magnetically isolated ones, are close to one another. The mutual magnetic interaction is high enough to smear the $^{51}V$ hyperfine structure but is not high enough to give rise to true coupled systems, the spectra of which are expected to be very different.

The two families of magnetically isolated V(IV) have a clear vanadylic character. This can be stated on the basis of the relatively high value of both $g_{iso}$ and $a_{iso}$ ($g_{iso} = (g_\parallel + 2\,g_\perp)/3$, $a_{iso} = (A_\parallel + A_\perp)/3$) which fall, according to the approach followed in (39, 40), in the region typical of the vanadyl groups. These vanadyl ions, furthermore, are stabilised at the surface (or near the surface) of the anatase $TiO_2$ phase and should have, in analogy with other well-defined species with similar spin-Hamiltonian parameters, a square pyramidal symmetry. This can be deduced on the basis of both a scrutiny of the literature data on $V_2O_5/TiO_2$ (40, 41, 42, and references therein) that evidences dramatic changes in the spectral shape according to the nature of the support (anatase, rutile, amorphous phases) and the location of vanadylic groups (surface, reticular, interstitial). Furthermore, a comparison of the spectrum of the $V_2O_5$–$WO_3/TiO_2$ sample (Fig. 4a) with that of a binary $V_2O_5/TiO_2$ reference sample (Fig. 4b) indicates that the single isolated species present in the binary sample is practically coincident with species I in Fig. 4a. The similarity of the $VO^{2+}$ ions present on the binary reference samples and on the ternary ones indicates that in these systems the vanadium oxide phase primarily interacts with titanium oxide. The difference between the binary and the ternary samples is, however, not only quantitative (different amounts of tetravalent vanadium) but also qualitative in that the ternary samples only show two families of vanadyl ions with similar but distinct spin-Hamiltonian parameters. The presence of two types of isolated vanadylic $VO^{2+}$ groups seems to be typical of the investigated ternary systems.

The role and even the presence in significant amounts of V(IV) in the vanadia monolayer of $TiO_2$-supported systems have been the object of a long debate in the literature. While several authors, on the basis of EXAFS, TPR, and XPS data (43–46), concluded that pentavalent vanadium is the only component of the overlayer on $TiO_2$, other authors showed the presence of nonnegligible amounts of vanadium(IV) (47, 48, 49). The existence of both V(IV) and V(V) is in line with the data of Jonson *et al.* (50), who refer to $V^{4+}$–$V^{5+}$ as the active redox couple in vanadia/titania samples.

The highly sensitive EPR technique has been quite extensively used in the study of vanadia/titania systems and a quite large number of papers are available that report EPR spectra of V(IV) on various, and variously treated, $V_2O_5/TiO_2$ systems (42 and references therein, 51–54). This technique, is not widely used for quantitative measurements. Accordingly, while the presence of V(IV) in $V_2O_5/TiO_2$ is generally accepted, its quantitative evaluation by EPR is not an easy task and has been attempted, to our knowledge, only by Rusiecka *et al.* (53), who reported some 6% V(IV) in a vanadia on anatase sample with 1.2% $V_2O_5$ loading. Taking into account the poor accuracy of the EPR quantitative measurements, this value can be considered in agreement with data indicating roughly 15% V(IV) derived with analytical titrimetric methods by the same group (55) and other authors (54).

An explicit and precise evaluation by EPR of the content of V(IV) in the ternary $V_2O_5$–$WO_3/TiO_2$ is not among the aims of the present paper. However, preliminary comparison of the spectral intensity of the ternary system with those of frozen solutions of vanadyl acetilacetonate in toluene shows that the observed V(IV) should be around 8–10% of the total vanadium in the samples. This result indicates that despite the observation that V(IV) is a minor fraction of the total vanadium in the system, its concentration can be considered high enough for an adequate probe of the structural features of the V ions anchored at the surface. A further difference between ternary and binary $V_2O_5/TiO_2$ samples is observed upon outgassing at 823 K. After this treatment the tuning of

the spectrometer was practically impossible in the case of $V_2O_5$–$WO_3/TiO_2$ (and of $TiO_2$ and $WO_3/TiO_2$ as well) because the concentration of quasi-free electrons in the samples exceeded a limiting value. By comparison, in the case of $V_2O_5/TiO_2$ samples the EPR spectra could be monitored even after outgassing at this temperature.

### 4. *UV–vis Diffuse Reflectance*

*4.1. Calcined samples.* The UV–vis DR spectra of $TiO_2$, $WO_3/TiO_2$, $V_2O_5/TiO_2$, and $V_2O_5$–$WO_3/TiO_2$ samples are presented in Fig. 5.

The spectrum of pure $TiO_2$ is dominated by the edge relative to the $O^{2-} \rightarrow Ti^{4+}$ charge transfer to $TiO_2$ anatase at 320–350 nm.

The $WO_3/TiO_2$ sample shows an additional broad absorption near 430 nm. This absorption is responsible for the pale yellow color of the samples and it can be due to $O^{2-} \rightarrow W^{6+}$ charge transfer transition, as in the case of monoclinic $WO_3$ (56), or to a perturbation of the $TiO_2$ edge by surface tungsten oxide species. The absence of significant absorptions in the visible region due to *d–d* transition points to the absence of reduced W species with respect to the $d^0$ hexavalent state of $W^{6+}$.

The spectra of $V_2O_5/TiO_2$ samples show a strong additional absorption at 410 nm and an additional absorption in the whole visible region with maximum at 670 nm; both absorptions increase with $V_2O_5$ loading. These bands have been associated with the presence of $V^{4+}$ in the form of $VO^{2+}$ species (9); the band at 410 nm can also be explained as due to a perturbation of the $TiO_2$ edge by surface vanadium oxide species.

The spectra of $V_2O_5$–$WO_3/TiO_2$ samples show absorptions at 410 and 520 nm and an absorption extending in the whole visible region. All of these absorptions are more intense in $V_2O_5$–$WO_3/TiO_2$ samples than in $WO_3/TiO_2$ and $V_2O_5/TiO_2$ samples with similar metal loadings. The intensity of the absorption at 520 nm, with $WO_3/TiO_2$ as a reference, increases linearly with the $V_2O_5$ content up to the (W + V) monolayer coverage value ($V_2O_5 \sim 2.5\%$ w/w), as shown in Fig. 6. This absorption in principle can be associated either with *d–d* transitions of reduced V and/or W cations or with a $O^{2-} \rightarrow V^{5+}$ charge transfer. The absorption in the visible region is similar to that found on reduced $TiO_2$ (57) and is due to the presence of quasi-free electrons. However, that all these features are higher in intensity in $V_2O_5$–$WO_3/TiO_2$ than in the corresponding $WO_3/TiO_2$ and $V_2O_5/TiO_2$ samples indicates that a specific electronic interaction occurs between W and V oxide species, possibly involving the support.

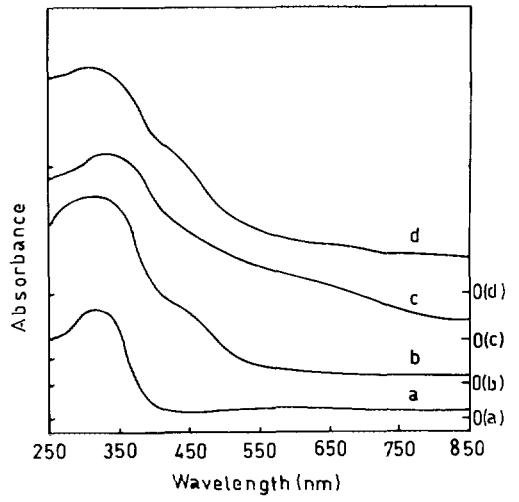


FIG. 5. UV–vis DR spectra of calcined $TiO_2$ (a), $WO_3(9)/TiO_2$ (b), $V_2O_5(1.4)/TiO_2$ (c), and $V_2O_5(1.4)$–$WO_3(9)/TiO_2$ (d), with $BaSO_4$ as reference.

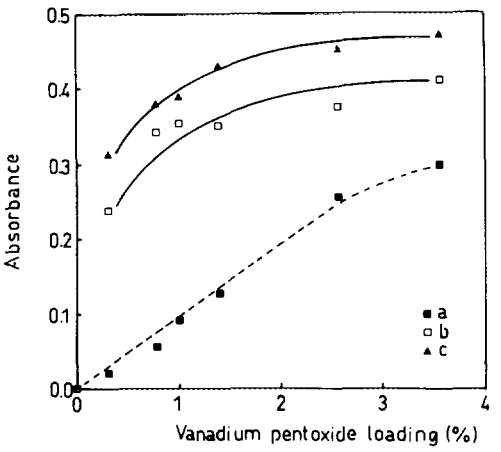


FIG. 6. Intensity of the absorptions at 520 nm in UV–vis DR spectra as a function of the $V_2O_5$ content for calcined (a) and reduced $V_2O_5$–$WO_3/TiO_2$ samples after 16 h outgassing (b) and 32 h outgassing (c). The spectra were taken with $WO_3/TiO_2$ as reference.

*4.2. Outgassed samples.* The UV–vis DR spectra of $V_2O_5$–$WO_3/TiO_2$ samples outgassed for 16 h and 32 h were recorded *in situ* at r.t. The color of the samples was much darker (almost black), and absorptions more intense than in the case of the calcined samples were measured in the whole visible region and particularly at 520 nm (Fig. 6). Under the same experimental conditions. The additional absorption extending in the whole visible region was observed to a much lower extent in the case of $WO_3/TiO_2$ (with a broad maximum at 530 nm) and to an even lower extent in the case of $TiO_2$; it has not monitored for the correspondent $V_2O_5/TiO_2$ samples.

These results are in line with the previous interpretation of the above absorptions as due to the presence of quasi-free electrons and to *d–d* transitions of reduced V and/or W oxide species. The growth of these absorptions upon outgassing of the ternary catalysts can be explained by a reduction of the catalyst. It is in fact well known that

$TiO_2$ increases its *n*-type semiconductor properties due to oxygen deficiency upon reduction and/or outgassing (e.g., at 673 K and $10^{-4}$ Torr for 1 h) [57]. Reduced titanium oxides have been characterised recently and are found to be dark in colour and to present a continuous absorption in the visible region [58] as well as a higher absorption in the IR region (57). These absorptions are likely due to transitions involving nearly free electrons, i.e., electrons placed in delocalised orbitals or in the conduction band. At low temperature (e.g., 77 K) the electrons can be trapped in localized orbitals, originating typical EPR signals of $Ti^{3+}$. $WO_3/TiO_2$ presents a similar behavior whereas $V_2O_5/TiO_2$ shows a higher tendency to localise electrons at vanadium centers, giving rise to $V^{4+}$ ions. The behavior of $V_2O_5$–$WO_3/TiO_2$ is similar to that of $WO_3/TiO_2$ but shows an easier reducibility. Besides, when the temperature and/or the degree of reduction are low the electrons are essentially trapped at vanadium centers.

### 5. *Vibrational Studies*

The FTIR spectra in Fig. 7 and the Laser Raman spectra in Fig. 8 of the supported species arising from $V_2O_5$ and $WO_3$ components in the ternary and binary catalysts are

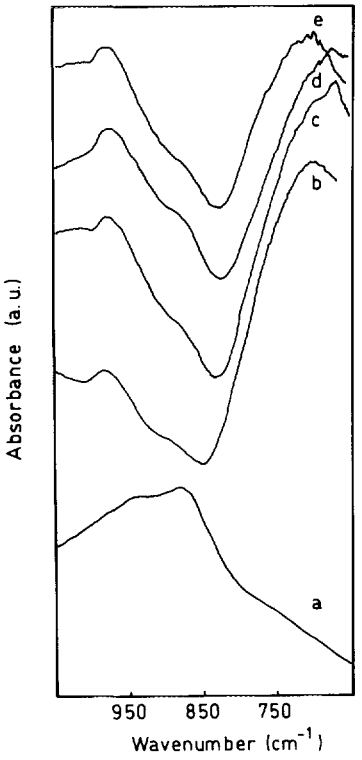


FIG. 7. FTIR spectra of the supported phases (KBr pressed disks, support spectrum subtracted) of $V_2O_5(1.4)/TiO_2$ (a), $WO_3(9)/TiO_2$ (b), $V_2O_5$–$WO_3(9)/TiO_2$ samples with $V_2O_5$ = 0.3% w/w (c), 1.0% w/w (d), and 1.4% w/w (e).

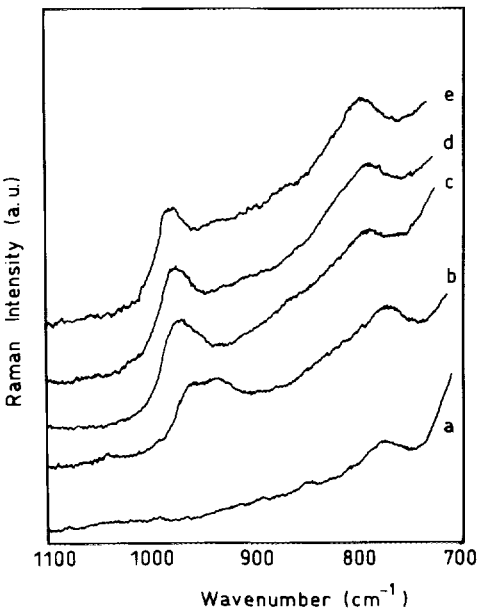


FIG. 8. Laser Raman spectra of calcinated $TiO_2$ (a), $V_2O_5(1.4)/TiO_2$ (b), $WO_3(9)/TiO_2$ (c), $V_2O_5(0.3)$–$WO_3(9)/TiO_2$ (d), and $V_2O_5(1.4)$–$WO_3(9)/TiO_2$(e).

reported in the 1100–700 $cm^{-1}$ range. The IR spectra (Fig. 7) have been taken in contact with air and KBr pressed disks and the spectrum of the $TiO_2$ support has been subtracted. The Raman spectra (Fig. 8) have been taken in air using the pure powders. In this spectral region the pure anatase support absorbs strongly below 800 $cm^{-1}$ but does not show any IR maximum down to 450 $cm^{-1}$. In the Raman spectra of anatase $TiO_2$ only a weak overtone is detected at 790 $cm^{-1}$ (Fig. 8a). Figure 9 shows the FTIR spectra of pure powder pressed disks of the binary and ternary catalysts after outgassing at 573 K. The spectrum of the $TiO_2$ support has been subtracted in this case also.

The IR spectra of the binary $V_2O_5/TiO_2$ catalysts corre-

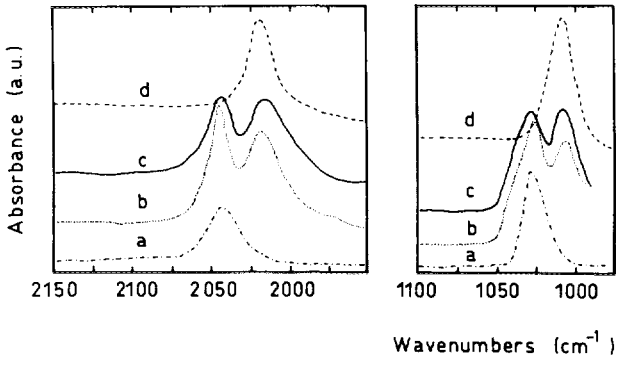


FIG. 9. FTIR spectra of pure pressed disks after outgassing at 573 K for 15 min. Fundamental and overtone regions are shown. (a) $V_2O_5(1.4)/TiO_2$, (b) $V_2O_5(1.4)$–$WO_3(9)/TiO_2$, (c) $V_2O_5(0.3)$–$WO_3(9)/TiO_2$, and (d) $WO_3(9)/TiO_2$. The absorbance scales on the right are about 10 times those on the left.

spond to those already reported by our group (16, 17, 33, 59) and by other groups (14, 15, 18, 32). Two broad IR bands are found near 950 and 880 $cm^{-1}$. The Raman spectrum shows a broad peak, possibly split, with components near 980 and 950 $cm^{-1}$, and a very broad scattering in the region 950–700 $cm^{-1}$ with a maximum near 790 $cm^{-1}$ corresponding to the $TiO_2$ overtone peak cited above.

The higher frequency IR and Raman features (1000–940 $cm^{-1}$), the maximums of which shift slightly upwards on increasing the vanadium content, both in IR (33, 59) and in Raman (32), are assigned to the V=O stretching mode of vanadyl species in a hydrated form (16, 17). In dry conditions the same mode is observed at 1035 (fundamental) and 2045 $cm^{-1}$ (first overtone), with the former detectable also by Raman spectroscopy (16, 17, 32). The lower frequency features have been assigned to the highest frequency V–O stretching mode of metavanadate species (33). This assignment is based also on the Raman spectrum reported by Went *et al.* (15) in anhydrous conditions, which shows a sharper band in the region 915–930 $cm^{-1}$, and on a detailed analysis of the IR and Raman spectra of bulk Mg-vanadates (including Mg metavanadate), which show that metavanadate species are characterised mainly by V–O stretching modes responsible for a strong IR band at 888 $cm^{-1}$ and a strong Raman peak at 923 $cm^{-1}$ (60). So, the surface vanadium oxide species appear to be constituted essentially by monomeric vanadyl species and by metavanadate-type polymeric species. It is worth nothing that the coordination of vanadium in metavanadate species can change from essentially tetrahedral, like in ammonium metavanadate, to nearly octahedral, like in the "brannerite-type" metavanadates (as $MgV_2O_6$).

The data and assignments discussed above substantially agree with those already reported by Wachs and co-workers (26, 32, 61), Bell and co-workers (14, 15, 18), and other authors (45, 62) using Raman spectroscopy; they also agree with those reported by a number of authors using IR spectroscopic techniques (11, 47, 63–67).

The IR spectrum of the $WO_3/TiO_2$ sample in ambient conditions shows a relatively weak absorption near 980 $cm^{-1}$ and a much stronger one near 700 $cm^{-1}$. The corresponding Raman spectrum shows a prominent broad peak near 980 $cm^{-1}$ and a very broad scattering at lower frequencies, with a peak maximum at 800 $cm^{-1}$. According to Vuurman *et al.* (32) this second maximum grows strongly as a function of tungsten loading and should consequently be associated with surface tunsten oxide species. According to previous data (20) the peaks at 980 $cm^{-1}$ in both IR and Raman spectra are associated to the W=O stretching of wolframyl species. This mode is detected near 1015 $cm^{-1}$ by both IR and Raman spectroscopies (32) in the case of outgassed dry samples, when the wolframyl species are in a dehydrated form. The lower frequency modes (800 $cm^{-1}$ in the Raman spectrum, 700 $cm^{-1}$ in IR) are associated to W–O stretching modes of structures similar to $WO_3$ or their hydrates, like $WO_3 \cdot H2O$ (68). The position of these bands, according to the data collected by Stencel (69), should correspond to species where tungsten is in an octahedral environment with no W=O double bonds (as in the case of $WO_3$ polymorphs too). These species are also likely to be associated with weak Raman peaks observed at the lower frequencies, typically associated with deformation modes of W–O–W bonds, i.e., at 324 and 273 $cm^{-1}$.

The IR spectra of the ternary $V_2O_5$–$WO_3/TiO_2$ samples are similar to those of the binary $WO_3$–$TiO_2$ samples, in line with the relatively high $WO_3$ content and the low $V_2O_5$ content. Accordingly, two main IR absorptions are evident at 980 $cm^{-1}$ and near 700 $cm^{-1}$, together with a broad absorption near 880 $cm^{-1}$ that is more pronounced at high V loadings. The Raman spectra of ternary $V_2O_5$–$WO_3/TiO_2$ samples show again a broad peak at 980 $cm^{-1}$ and very broad scattering centered near 800 $cm^{-1}$. The higher frequency IR and Raman features are both associated with W=O and V=O stretchings of monomeric wolframyl and vanadyl species that are superimposed on each other. We note that the band at 950 $cm^{-1}$ associated with the V–O stretching mode of metavanadate species, which is very evident in the $V_2O_5/TiO_2$ sample, is present in the ternary catalysts as a shoulder because in wet conditions it is partially covered by the W=O and V=O stretchings of monomeric wolframyls and vanadyls.

Interestingly, when the samples are outgassed the V=O and W=O stretching modes split clearly (see Fig. 9 for the IR fundamental and overtone modes) and their positions are virtually the same as in binary $V_2O_5/TiO_2$ and $WO_3/TiO_2$ samples, respectively. This datum was interpreted by us as evidence of the mutual vibrational and structural independence of isolated vanadyl and wolframyl centers (30, 70) and it has also been confirmed by Vuurman *et al.* (32) using Raman spectroscopy in dry conditions. In the IR spectra, the lower frequency features in ternary systems are similar to those observed in binary $WO_3/TiO_2$ and should be taken as evidence of the presence of polymeric wolframate species. Also, we note that for the sample with higher $V_2O_5$ loading ($V_2O_5(1.4)$–$WO_3(9)/TiO_2$) the IR band near 700 $cm^{-1}$ shifts slightly towards higher frequencies upon increasing the vanadia content. This could be interpreted by hypotizing the formation of mixed $W_xV_yO_z$ polymeric species. In fact, the presence of vanadium in $W_xV_yO_z$ polymeric species can result in a shift of metal–oxygen stretching modes as compared to $W_xO_y$ species, due to its lower molecular weight. The low-frequency modes near 320 and 270 $cm^{-1}$ (see above) are apparently not affected by vanadium.

Another interesting feature is the presence of a weak absorption with a maximum near 880 $cm^{-1}$ that is more evident in the samples with higher vanadium content. This

feature could be due to small amounts of metavanadate species.

Additional information can be obtained by comparing the FT-Raman spectra of the pure support and of the binary and ternary samples in the overall spectral region (1200–100 $cm^{-1}$). In Fig. 10 the FT-Raman spectra of the support $TiO_2$ and of the $V_2O_5/TiO_2$, $WO_3/TiO_2$, and $V_2O_5$–$WO_3/TiO_2$ catalysts are shown for before and after outgassing at 473 K for 3 h. The features assigned above to surface vanadium oxide and tungsten oxide species (essentially centered in the ranges 1000–700 $cm^{-1}$ and 350–250 $cm^{-1}$) will not be evidenced or discussed further. The support spectrum shows five peaks at 638, 515, 396, 196, and 143 $cm^{-1}$, due to the six Raman active fundamentals of anatase, two of which are superimposed at 515 $cm^{-1}$ (71, 72). Outgassing only causes a slight weakening of the absolute peak intensity and a slight increase of the baseline at the high frequency side. The spectrum of the $V_2O_5(1.4)/TiO_2$ catalyst shows the same anatase peaks, without any shift but weakened by a factor near 7. Outgassing causes a further slight weakening of the anatase peaks and an increase of the baseline at the higher frequencies similar to that observed in the case of pure $TiO_2$. The spectrum of $WO_3/TiO_2$ shows the anatase peaks weakened by a factor 4.5. Outgassing causes a spectacular decrease in the intensity of the anatase peaks by a factor 12 and the line base shows an increase similar to the previous ones, emphasized by the scale expansion in the figure. The spectrum of the ternary oxide $V_2O_5(1.4)$–$WO_3(9)/TiO_2$ again shows the anatase peaks but they are dramatically decreased, by a factor 100 in comparison with those with pure $TiO_2$. In the spectrum recorded after outgassing the anatase peaks almost disappear, but this is only in part due to a further decrease in their intensity (which is almost constant); it is also due to an increase of the Raman scattering baseline.

The above Raman experiments provide evidence for three effects that are at least partially independent of each other, namely:

(i) The decrease in the anatase peak intensities in supported metal oxides is observed in all cases but most pronounced in the case of the $V_2O_5(1.4)$–$WO_3(9)/TiO_2$ catalyst. This effect, first reported for $V_2O_5/TiO_2$ (45) has also been found to be very pronounced in the cases of $MoO_3/TiO_2$ and $CuO/TiO_2$ (72) and much weaker, but significant, in the case of $SiO_2/TiO_2$ samples (73).

(ii) The anatase peak intensities decrease upon outgassing; the decrease is most evident in the case of the $WO_3/TiO_2$ catalyst. A complete loss of Raman scattering by reduction has been reported previously for rutile (74).

(iii) The increase of the Raman scattering baseline by outgassing is observed and is again most evident for the ternary catalysts.

This last effect can be associated with the appearance of broad absorption bands also in the IR spectra upon outgassing. Indeed for all the investigated catalysts (including $TiO_2$) outgassing at 573 K causes the almost complete loss of light transmission by the sample in the region below 3000 $cm^{-1}$, which is restored completely upon calcination. This effect is similar on all the above catalysts

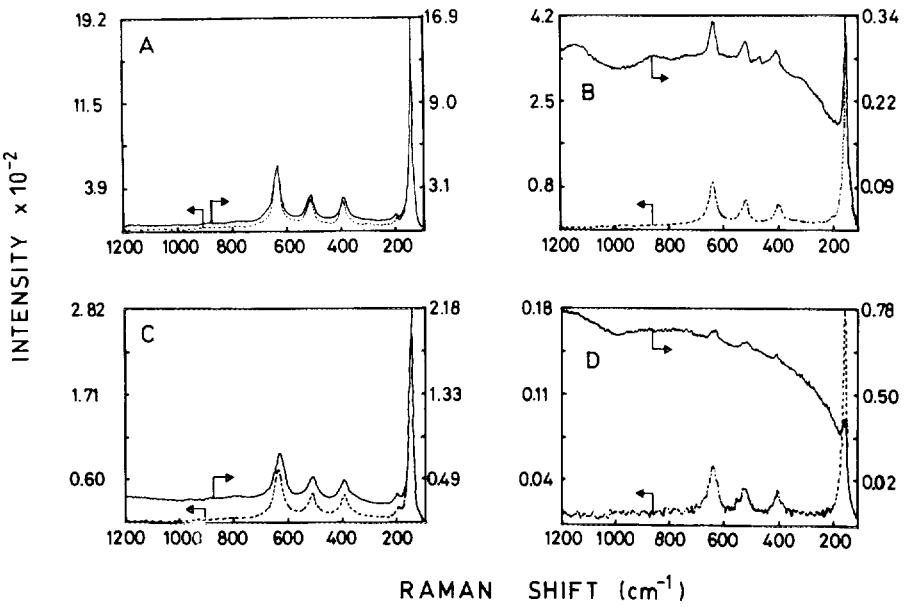


FIG. 10. FT-Raman spectra of calcined (dotted lines) and outgassed (solid lines) $TiO_2$ (A), $WO_3(9)/TiO_2$ (B), $V_2O_5(1.4)/TiO_2$2 (C), and $V_2O_5(1.4)$–$WO_3(9)/TiO_2$ (D).

but it occurs at much lower temperatures when W is present. This absorption necessarily involves the promotion of some electrons to the $TiO_2$ conduction band.

As for the first two effects, it is known that Raman scattering can be weakened (or broadened) and even lost due to the following different factors:

(i) Increased disorder. Indeed, the strength and sharpness of the Raman scattering peaks in bulk powders have been related by some authors to their degree of crystallinity (76). The possible role of surface disorder on "monolayer" catalyst surfaces in reducing Raman scattering has already been proposed by some of us (72, 73) but it is certainly not sufficient to explain the strong effects observed in the present cases.

(ii) Increased absorption of the exciting radiation is observed, with a consequent decrease in the intensity of the (Raman) scattered light (75). This also leads to temperature broadening that arises from heating due to the increased absorption of the exciting radiation. Working with a visible (Ar) laser, Bond and co-workers (45) first reported the effect of weakening the anatase Raman peaks in the case of $V_2O_5/TiO_2$ catalysts and attributed it to the increased absorption of the laser light with increased $V_2O_5$ content. However, this effect is observed using both a visible laser (Ar) and the near-IR laser (Nd YAG) of FT-Raman instruments. This effect does not seem strictly or solely correlated to the absorption of the laser light because, while $CuO–TiO_2$ and $V_2O_5/TiO_2$ (both of which show this strong effect) also absorb more than $TiO_2$ in the NIR region, this is not the case for calcined $WO_3/TiO_2$ or $SiO_2/TiO_2$ (which show this effect too, although it is weaker). Moreover, calcined $V_2O_5$–$WO_3/TiO_2$ catalysts, with which this effect is most pronounced, do not absorb more than $V_2O_5–TiO_2$ in the NIR region.

(iii) More complex solid-state phenomena like phonon–plasmon couplings.

## DISCUSSION

The results in Fig. 1 and Table 1 show that the presence of large amounts of tungsten (~9% w/w) are essential to preserve the structural and morphological properties of $WO_3/TiO_2$ samples upon addition of vanadia, provided that the (W + V) surface coverage is lower than one. In this case the samples are monophasic and consist of the anatase polymorphic form of $TiO_2$. Traces of rutile and $V_2O_5$, but not $WO_3$ or bulk $V_2O_5/WO_3$, are detected upon increasing the calcination temperature above 823 K and for high vanadia loadings, when the (W + V) coverage is close to or larger than that of the theoretical monolayer. On the other hand, when the $WO_3$ loading is kept low, a significant sintering of the catalyst is observed upon addition of $V_2O_5$.

The structure of the vanadium and tungsten oxide surface species present over the ternary $V_2O_5$–$WO_3/TiO_2$ catalysts with high tungsta content (~9% w/w) has been investigated by FTIR and laser Raman spectroscopies. Monomeric vanadyls and wolframyls, similar to those present on the surface of the binary oxide systems with comparable metal loadings, are observed over the samples with low $V_2O_5$ loadings. Indeed the positions of the V=O and W=O stretching modes in the ternary catalysts are virtually the same as in the binary $V_2O_5/TiO_2$ and $WO_3/TiO_2$ samples, respectively. The fundamental $\nu$(V=O) stretching mode is detected at 980 $cm^{-1}$ in wet conditions and at 1030 $cm^{-1}$ in dry conditions in both the IR and Raman spectra, and the first overtone $2\nu$(V=O) is observed at 2045 $cm^{-1}$ in dry conditions in IR spectra. The $\nu$(W=O) stretching mode is monitored at 980 $cm^{-1}$ in wet conditions and near 1020 $cm^{-1}$ in dry conditions in both IR and Raman spectra, and the first overtone $2\nu$(W=O) is observed at 2020 $cm^{-1}$ in dry conditions in the IR spectra. These results confirm the mutual structural and vibrational independence of the isolated vanadyl and wolframyl centers in the ternary catalysts. In addition to monomeric vanadyls and wolframyls the presence of polymeric $W_xO_y$ species, similar to those observed in the binary $WO_3/TiO_2$ sample, is revealed by the IR band near 700 $cm^{-1}$ and by the Raman bands at 800, 324, and 273 $cm^{-1}$. On increasing the vanadium content, polyvanadate species are also formed, characterised by the IR band at 880 $cm^{-1}$ and the Raman band at 950 $cm^{-1}$. Besides, slight evidence for the presence of mixed $W_xV_yO_z$ species, where Vanadium is dispersed within the W–O–W chains of $W_xO_y$, comes from the shift towards higher frequency observed for the IR band associated with $W_xO_y$ species and observed at 700 $cm^{-1}$ in $WO_3/TiO_2$. The formation of the mixed $W_xV_yO_z$ species implies a structural interaction between V and W centers over the $TiO_2$ surface.

Additional structural information on the surface V species comes from EPR spectroscopy. Preliminary quantitative evaluation by EPR indicates that 8–10% of the total vanadium in the ternary samples is present as V(IV), which appears to be enough for an adequate probe of the structural features of the reduced ions anchored at the surface of the support. The tetravalent vanadium ions are present in vanadyl forms, as indicated by the $g$ and $A$ values discernable from the EPR spectra; two families of magnetically isolated vanadylic ions and more clustered magnetically interacting ions are present at the surface. The spin-Hamiltonian parameters of isolated species suggest that the vanadylic ions are primarily stabilised through interaction with the titania surface rather than with the tungsta. However, only one of the two families of isolated $VO^{2+}$ ions present in the ternary samples has been observed over the binary $V_2O_5–TiO_2$ samples. These results suggest that in spite of the structural and vibra-

tional independence of the isolaed V and W surface species present in the ternary $V_2O_5$–$WO_3/TiO_2$ samples, tungsta plays a role in determining both the amount and the properties of the surface vanadyl ions in the ternary catalysts.

EPR, UV–vis, and laser-Raman spectroscopies converge in indicating a strong electronic interaction between V and W oxide surface species and the $TiO_2$ support. Indeed, $WO_3/TiO_2$ easily loses oxygen by outgassing and, when slightly reduced, shows the typical behavior of an *n*-type semiconductor, i.e., quasi-free electrons, easily promoted to the $TiO_2$ conduction band, are produced. This interpretation is supported by the detection of a broad absorption extending from the UV to the IR region, by the impossibility of recording EPR spectra in the case of outgassed $WO_3/TiO_2$, and by the increase of the Raman scattering baseline upon outgassing due to excessive amounts of quasi-free electrons. The same phenomena occurs, but only under much more drastic conditions, in the case of pure $TiO_2$. On the contrary, V centers in slightly reduced $V_2O_5/TiO_2$ seem to trap electrons, giving rise to $V^{4+}$ centers, well-evidenced by EPR and possibly by the *d–d* absorptions essentially localised in the UV–visible regions. When $V_2O_5$ is added to $WO_3/TiO_2$ the production of quasi-free electrons is already made easier on calcined samples, and it becomes even more so after outgassing so that the EPR spectra cannot be recorded, a strong absorption extending in the whole visible region is observed, and the anatase Raman peaks are very strongly weakened. This electronic interaction eventually accounts for a greater reducibility of the ternary samples as compared to the binary ones so that the EPR spectra of the calcined ternary samples are more intense by one order of magnitude.

The $V_2O_5$–$WO_3/TiO_2$ catalysts exhibit higher reactivity in the selective catalytic reduction of NO by $NH_3$ than the corresponding binary $V_2O_5/TiO_2$ catalysts; the ternary catalysts are active at lower temperatures and high selectivities to $N_2$ are preserved in the high-temperature region. As a result, the temperature window for the SCR reaction, corresponding to high $NO_x$ conversion and complete selectivity to $N_2$, is greatly widened. Calculations have shown that the reactivity of V and/or W over the ternary samples, identified in terms of specific rates of reaction according to Eq. [1], is greater than that measured over the corresponding binary system, which eventually indicates the existence of a synergism between V and W oxide species in the SCR reaction.

Although the formation of larger amounts of highly reactive polyvanadate species in the ternary samples, due to the decrease in the $TiO_2$ surface area which is available for vanadium, is neither confirmed nor excluded by our vibrational study, calculations indicate that this does not fully account for the increase in the catalytic activity. Furthermore, the presence of highly reactive polyvanadate species is also accompanied by lower selectivity to $N_2$ in the SCR reaction (18, 19), which, however, is not observed over the $V_2O_5$–$WO_3/TiO_2$ catalysts.

The higher reactivity of the ternary catalysts can be associated with the existence of strong electronic interactions between V and W oxide surface species revealed by EPR, UV–vis and Raman spectroscopies. In fact, it has been observed that this leads to a different reducibility of the samples. Along these lines, recent TPSR/TPR experiments performed in our laboratories in the presence and in the absence of oxygen confirmed that the ternary catayst can be reduced at lower temperatures, due to the participation of labile lattice oxygen atoms in the $DeNO_x$ SCR reaction, and can be reoxidized more easily by gaseous oxygen (77). Accordingly, the higher reactivity of the ternary catalysts with respect to the corresponding binary samples can be related to their superior redox properties.

The electronic interaction between V and W oxide surface species may occur through oxygen bridging of the polyhedra and/or through the conduction band of $TiO_2$. The former possibility is consistent with the formation of mixed $W_xV_yO_z$ species and with the detection of relatively isolated $VO^{2+}$ ions that are slightly different from those monitored over $V_2O_5/TiO_2$ by EPR. Considering that the active sites for $SO_2$ oxidation have been envisaged as dimeric vanadyls and that this reaction is favoured by high degrees of oxidation of the active sites (4), a more controlled extent of reduction of the V oxide species and/or the dispersion of vanadium ions within polymeric $W_xO_y$ groups at the surface of titania may likely account for low conversions in $SO_2$ oxidation and for high activities in $NO_x$ reduction as well. These catalytic properties are indeed common to all commercial $DeNO_x$ SCR catalysts.

Other factors, however, must be considered when comparing the reactivities in the SCR reaction of the ternary and binary catalysts. For example, several authors assign Brønsted acid sites a pivotal role in the $DeNO_x$ reaction (78 and references therein). There is no doubt that the addition of tungsten significantly increases the surface acidity of $V_2O_5/TiO_2$ catalysts. This was also confirmed by recent TPSR and TPR experiments performed over the catalysts used in the present work (77). However, as pointed out by the catalytic activity runs shown in Fig. 2, the ternary samples already show significant activity at low temperatures, where the reactivity of the samples is not controlled by adsorbed ammonia but is likely governed by the mobility of the catalyst lattice oxygen. Thus it is believed that the catalyst redox properties, rather than surface acidity, is the factor that controls the reactivity of the samples, at least at low temperatures. However, at

high temperatures the surface acidity certainly plays an important role in the adsorption and activation of ammonia.

## CONCLUSIONS

The following main conclusions have been obtained in the present study performed over $V_2O_5$–$WO_3$/$TiO_2$ $DeNO_x$ catalysts:

(i) Monophasic materials with high surface areas are obtained for large tungsta contents ($WO_3$ = 9% w/w) and (V + W) surface coverages lower than one ($V_2O_5$ < 2.56% w/w).

(ii) Monomeric vanadyls and wolframyls and polymeric $W_xO_y$ groups are observed in the submonolayer samples and are apparently similar to those observed over the binary catalysts. Polyvanadate species are also observed at high vanadia contents. Mixed $W_xV_yO_z$ species, where vanadium is dispersed within the W–O–W chains of $W_xO_y$, and relatively isolated $VO^{2+}$ ions slightly different from those monitored over $V_2O_5$/$TiO_2$ are also observed in the ternary catalysts.

(iii) A strong electronic interaction operates between V and W oxide surface species and the $TiO_2$ support, which results in a higher reducibility of the ternary catalysts with respect to the corresponding binary samples. The electronic interactions lead the formation of free electrons and may operate through oxygen bridging of the polyhedra and/or through the conduction band of the anatase $TiO_2$ support.

(iv) The ternary catalysts are more active than the corresponding binary ones because a synergism operates between V and W oxide species in the SCR reaction. This can be eventually related to the strong electronic interactions between V and W oxide surface species and the $TiO_2$ support and, accordingly, to the higher reducibility of the ternary samples.

## ACKNOWLEDGMENTS

This work was performed under contract with ENEL/DSR/CRTN Milano. The financial support of CNR-attività di comitato is also acknowledged.

## REFERENCES

1. Bosch, H., and Janssen, F., *Catal. Today* **2,** 369 (1988).
2. Inomata, M., Mori, K., Myiamoto, A., Ui, T., and Murakami, Y., *J. Phys. Chem.* **87,** 754 (1983).
3. Svachula, J., Ferlazzo, N., Forzatti, P., Tronconi, E., and Bregani, F., *Ind. Eng. Chem. Res.* **32,** 1053 (1993).
4. Svachula, J., Alemany, L. J., Ferlazzo, N., Forzatti, P., Tronconi, E., and Bregani, F., *Ind. Eng. Chem. Res.* **32,** 826 (1993).
5. Andersson, A., and Andersson, S. L. T., *in* "Solid State Chemistry in Catalysis" (R. K. Grasselli and J. F. Brazdil, Eds.), p. 121. ACS, Washington, 1985.
6. Gellings, P. J., *in* "Catalysis," Vol. 7, p. 105. Royal Society of Chemistry, London, 1985.
7. Haber, J., Kozlowska A., and Kozlowski, R., *J. Catal.* **102,** 52 (1986).
8. Vejoux A., and Courtine, P., *J. Solid State Chem.* **63,** 179 (1986).
9. Busca, G., Tittarelli, P., Forzatti, P., and Tronconi, E., *J. Solid State Chem.* **67,** 91 (1987).
10. Cavani, F., Foresti, E., Parrinello, G., and Trifirò, F., *Appl. Catal.* **38,** 311 (1988).
11. Hausinger, G., Schmelz, H., and Knozinger, H., *Appl. Catal.* **39,** 267 (1988).
12. Bond, G. C., Flamers, S., and Shukri, R., *Faraday Discuss. Chem. Soc.* **87,** 65 (1989).
13. Eckert, H., and Wachs, I. E., *J. Phys. Chem.* **93,** 6796 (1989).
14. Went, G. T., Oyama, S. T., and Bell, A. T., *J. Phys. Chem.* **94,** 4240 (1990).
15. Went, G. T., Leu, L.-J., and Bell, A. T., *J. Catal.* **134,** 479 (1992).
16. Cristiani, C., Busca, G., and Forzatti, P., *J. Catal.* **116,** 586 (1989).
17. Ramis, G., Cristiani, C., Forzatti, P., and Busca, G., *J. Catal.* **124,** 574 (1990).
18. Went, G. T., Leu, L.-J., Rosin, R. R., and Bell, A. T., *J. Catal.* **134,** 492 (1992).
19. Lietti, L., and Forzatti, P., *J. Catal.* **147,** 241 (1994).
20. Ramis, G., Busca, G., Cristiani, C., Lietti, L., Forzatti, P., and Bregani, F., *Langmuir* **8,** 1744 (1992).
21. Cristiani, C., Bellotto, M., Forzatti P., and Bregani, F., *J. Mater. Res.* **8,** 2019 (1993).
22. Lietti, L., Svachula, J., Forzatti, P., Busca, G., Ramis, G., and Bregani, F., *Catal. Today* **17,** 131 (1993).
23. Bell, A. T., and Carberry, J. J., *Catal. Rev. Sci. Eng.* **27,** 1 (1985).
24. Hilbrig, F., Schmelz, H., and Knozinger, H., *in* "New Frontiers in Catalysis" (L. Guczi, F. Solymosi, P. Téténi, Eds.), p. 1351. Elsevier, Amsterdam/New York, (1993).
25. Bond, G. C., Flamerz, S., and Wan Wijk, L., *Catal. Today* **1,** 229 (1987).
26. Wachs, I. E., and Hardcastle, E., "Proceedings, 9th International Congress on Catalysis, Calgary, 1988," (M. J. Philips and M. Ternan, Eds.), Vol. 3, p. 1449. Chem. Institute of Canada, Ottawa, 1988.
27. Imanari, I., Watanabe, Y., Matsuda, S., and Nakajima, F., "Proceedings, 7th International Congress on Catalysis, Tokyo 1980" (T. Seiyama and K. Tanabe, Eds.), Elsevier, Amsterdam, 1981.
28. Hilbrig, F., Gobel, H. E., Knozinger, H., Schmelz, H., and Lengeler, B., *J. Phys. Chem.* **95,** 6973 (1991).
29. Morikawa, S., Takahashi, K., Mogi, J., and Kurita, S., *Bull. Chem. Soc. Japan* **55,** 2254 (1982).
30. Ramis, G., Busca, G., and Forzatti, P., *Appl. Catal. B Environ.* **1,** L9–L13, (1992).
31. Chen, J. P., and Yang, R. T., *Appl. Catal. A Gen.* **80,** 135 (1992).
32. Vuurman, M. A., Wachs, I. E., and Hirt, A. M., *J. Phys. Chem.* **95,** 9982 (1991).
33. Lietti, L., Forzatti, P., Ramis, G., Busca, G., and Bregani, F., *Appl. Catal. B Environ.* **3,** 13 (1993).
34. Deo, G., and Wachs, I. E., *J. Catal.* **146,** 335 (1994).
35. Deo, G., and Wachs, I. E., *J. Catal.* **146,** 323 (1994).
36. Vermaire, D. C., and van Berge, P. C., *J. Catal.* **116,** 309 (1989).
37. Bond, G. C., and Tahir, S. F., *Appl. Catal.* **71,** 1 (1991).
38. Wong, W. C., and Nobe, K., *Ind. Eng. Chem. Prod. Res. Dev.* **23,** 564 (1984).
39. Goodman, B. A., and Raynor, J. B., *Adv. Inorg. Chem. Radiochem.* **13,** 188 (1970).

40. Davidson, A., and Che, M., *J. Phys. Chem.* **96,** 9909 (1992).
41. Busca, G., Marchetti, L., Centi, G., and Trifirò, F., *Langmuir* **2,** 568 (1986).
42. Busca, G., and Giamello, E., *Mater. Chem. Phys.* **25,** 475 (1990).
43. Eckerdt, H., Wachs, I. E., *J. Phys. Chem.* **93,** 6796 (1989).
44. Kozlowski, R., Pettifer, R. F., and Thomas, J. M., *J. Phys. Chem.* **87,** 5176 (1983).
45. Bond, G. C., Zurita, J. P., Flamerz, S., Gelling, P. J., Bosch, H., van Ommen, J. G., and Kip, B. J., *Appl. Catal.* **22,** 361 (1986).
46. Eckerdt, H., Deo, G., Wachs, I. E., and Hirt, A. M., *Colloids Surf.* **45,** 347 (1990).
47. Turco, M., Bagnasco, G., Lisi, L., and Ciambelli, P., *J. Therm. Anal.* **38,** 2631 (1992).
48. Pereira, E., Gambaro, L. A. and Thomas, H. J., *Transition Met. Chem.* **5,** 139 (1980).
49. Andersson, S. L. T., *Catal. Lett.* **7,** 351 (1990).
50. Jonson, B., Rebenstorf, B., Larsson, R., and Andersson, S. L. T., *J. Chem. Soc. Faraday Trans. 1* **84,** 3547 (1988).
51. Mériaudeau, P., and Vedrine, J. C., *Nouv. J. Chim.* **2,** 133 (1978).
52. Gallay, R., van der Klink, J. J., and Moser, J., *J. Phys. Rev.* **34,** 3060 (1986).
53. Rusiecka, M., Grzybowska, B., *Appl. Catal.* **10,** 87 (1984).
54. Sanati, M., Wallenberg, R., Andersson, A., Jansen, S., and Tu, Y., *J. Catal.* **132,** 128 (1991).
55. Gasior, M., Gasior, I., and Grzybowska, B., *Appl. Catal.* **10,** 87 (1984).
56. Ramis, G., Cristiani, C., Elmi, A. S., Villa, P. L., Busca, G., *J. Mol. Catal.* **61,** 319 (1990).
57. Busca, G., and Zecchina, A., *Catal. Today* **3,** 61 (1994).
58. Ookubo, A., Kanezaki, E., and Ooi, K., *Langmuir* **6,** 296 (1990).
59. Oliveri, G., Ramis, G., Busca, G., and Sanchez Escribano, V., *J. Mater. Chem.* **3,** 1239 (1993).
60. Busca, G., Ricchiardi, G., Siew Hew Sam, D., and Volta, J. C., *J. Chem. Soc. Faraday Trans.* **90,** 1161 (1994).
61. Wachs, I. E., *J. Catal.* **124,** 570 (1990).
62. Roozenboom, F., Mittelmeijer-Hazeleger, M. C., Moulijn, J. A., Medema, J., DeBeer, V. H. J., and Gellings, P. J., *J. Phys. Chem.* **84,** 2783 (1980).
63. Andersson, A., *J. Catal.* **76,** 144 (1982).
64. Bond, G. C., and Konig, P., *J. Catal.* **77,** 309 (1982).
65. Schraml-Marth, M., Fluhr, W., Wokaun, A., and Baiker, A., *Ber. Bunsenges. Phys. Chem.* **8,** 852 (1989).
66. Ciambelli, P., Bagnasco, G., Lisi, L., Turco, M., Chicarello, G., Musci, M., Notaro, M., Robba, D., and Ghetti, P., *Appl. Catal. B Environ.* **1,** 61 (1992).
67. Kantcheva, M. M., Hadjiivanov, K. I., and Klissurrski, D. G., *J. Catal.* **134,** 299 (1992).
68. Daniel, M. F., Desbat, B., Lassegues, J. C., Gerand, B., and Figlarz, M., *J. Solid State Chem.* **67,** 235 (1987).
69. Stencel, J. M., "Raman Spectroscopy for Catalysis," Van Nostrand–Reinhold, New York, 1990.
70. Ramis, G., Busca, G., and Bregani, F., *Catal. Lett.* **23,** 353 (1994).
71. Ohsaka, T., Izumi, F., and Fujiki, Y., *J. Raman Spectrosc.* **7,** 321 (1978).
72. Busca, G., Gallardo, Amores, J. M., Piaggio, P., Ramis, G., and Sanchez Escribano, V., *J. Chem. Soc. Faraday Trans.* **90,** 3181 (1994).
73. Yi, L., Ramis, G., Busca G., and Lorenzelli, V., *J. Mater. Chem.* **4,** 1755 (1994).
74. Ocana, M., Fornes, V., Garcia Ramos, J. V., and Serna, C. J., *J. Solid State Chem.* **75,** 364 (1988).
75. Waters, D. N., *Spectrochim. Acta* **50A,** 1833 (1994).
76. Hayashi, S., and Kanamori, K., *Phys. Rev. B* **26,** 7079 (1982).
77. Unpublished results from our laboratories.
78. Chen, J. P., and Yang, R. T., *J. Catal.* **139,** 277 (1993).